

Comparative Studies of WC-Co and WC-Co-Ni Composites Obtained by Conventional Powder Metallurgy

Vinícius Martins^a, Wilson Corrêa Rodrigues^a, Peterson Luiz Ferrandini^a, Denis Jardim Villarinho^a,

Gerhard Hans Knörschild^{b*}, Lirio Schaeffer^a

^aLaboratório de Transformação Mecânica – LdTM, Centro de Tecnologia, Universidade de Federal do Rio Grande do Sul – UFRGS, Av. Bento Gonçalves, n.º. 9500, CEP 91501-970, Porto Alegre, RS, Brazil

^bLaboratório de Processos Eletroquímicos e Corrosão – Eletrocorr, Universidade de Federal do Rio Grande do Sul – UFRGS, Av. Bento Gonçalves, n.º. 9500, CEP 91501-970, Porto Alegre, RS, Brazil

Received: March 18, 2011; Revised: May 9, 2011

The present work reports a comparative study of cemented carbides of compositions WC-6Co, WC-10Co, WC-20Co, WC-6Co-6Ni and WC-12Ni-6Co. The purpose was to study the powder metallurgical production process of these compositions starting from a commercial WC-6Co powder, obtaining the desired compositions by mass balance with pure Co and pure Ni powders. During the process steps mixing, milling, compacting and sintering the powders were described by its apparent density, green density, shrinkage and sintered density. Lower densities were observed in composites with higher binder content. The process was monitored by scanning electron microscopy and EDS analysis to evaluate the homogeneity of the powders, to detect contaminations by the process and to characterize the microstructure of the sintered materials. A finer microstructure was found when the binder contained Ni. Potentiodynamic polarization tests in sulfuric acid revealed pseudo-passive behavior for all the tested hard metals.

Keywords: powder metallurgy, hard metal, WC-Co, WC-Co-Ni

1. Introduction

Hard metals are essentially composed of WC particles incorporated in a Co matrix. Their characteristics are high hardness and wear resistance, resistance to compression, tenacity and thermal stability. The properties are defined by the combination of the properties of the carbides and of the matrix. Other carbide forming elements, present in many hard metals, are Ti, Ta, V, Nb. The addition of small quantities of these elements has the function to inhibit WC grain growth during sintering¹⁻⁵. WC dissolves in the Co matrix during sintering and precipitates again at other carbide particles during cooling. In this way particle coarsening occurs since small carbides dissolve preferentially and reprecipitate at greater particles. Together with the grain growth the morphology of the carbides changes¹. The carbon content is another important aspect which modifies the properties of hard metals. The carbon content has to be between 6.15 and 6.20 wt. (%), in the matrix phase between 0.10 and 0.18 wt. (%). Higher carbon contents cause reprecipitation of carbon as free graphite^{6,7}.

The role of Co in hard metals is to form a ductile matrix for the carbide particles. During liquid phase sintering it permits to obtain material of high density⁸. Commercial hard metals have a Co content between 3 and 25 wt. (%)⁹.

Due to the excellent wettability of WC by the liquid phase considerable contraction is observed during sintering at about 1300 °C. Solidification of Co occurs at about 1275 °C; during subsequent cooling about 4 wt. (%) of WC is retained in solution. At room temperature the dissolved WC in the Co binder is less than 1 wt. (%)^{10,11}.

Nickel, a ductile metal, is sometimes added to modify the binder composition. The most important aim of this modification with Ni is to improve the corrosion resistance of the hard metal¹².

In the present work the powder metallurgical production of WC-CoNi composites is documented, using as raw material a commercial WC-6Co powder. The influence of Ni on the different production steps is monitored by electron microscopy and EDS. The influence of Ni on the electrochemical behavior is examined by voltammetric curves.

2. Materials and Methods

Commercial WC-6%Co powder with purity of 99% and granulometry of -325 Mesh was delivered by Alfa Aesar. Powders of the pure metals, Co and Ni, (99% purity, -400 Mesh) were also delivered by Alfa Aesar.

Composites with the desired composition were obtained by mixing the commercial WC-6Co powder with the pure metal powders.

Using mass balance calculations the necessary quantities of Co and Ni were determined, which have to be added to 100 g of WC-6Co in order to obtain the following materials: 90WC-10Co, 80WC-20Co, 94WC-6Co, 88WC-6Co-6Ni, 82WC-6Co-12Ni. The calculated quantities of Co and Ni are listed in Table 1.

The powder mixture was prepared in two steps: At first the powder components were put in an attritor mill and mixed one hour at 100 rpm in ethylic alcohol under argon atmosphere. In the second step the powder mixture was homogenized during 30 minutes in a Y-mixer with the addition of 1.5 wt. (%) zinc stearate as lubricant.

*e-mail: gerhard.hans@ufrgs.br

After mixing the powders were pressed in a cylindrical matrix with a compacting pressure of 200 MPa.

Sintering was performed under argon atmosphere in a tubular furnace with electronic control and precision of ± 1 °C. A sintering cycle consisted of heating up to 580 °C at 5.8 °C/min, holding the temperature at 580 °C for 20 minutes. In the following heating continued with 8 °C/min up to the sintering temperature, which was held for 60 minutes. Afterwards the furnace was cooled down at a rate of 6 °C/min.

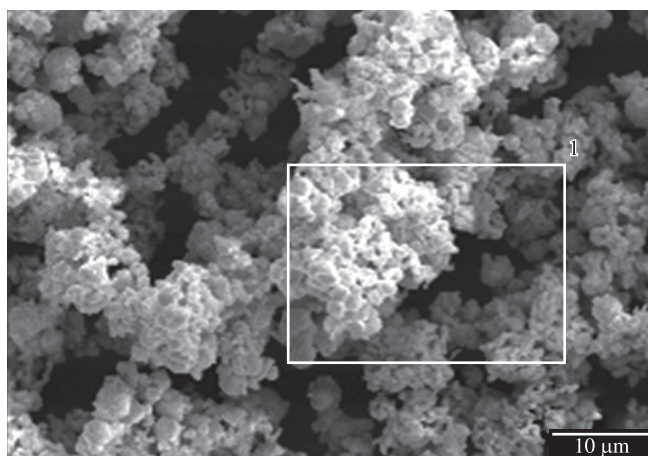
The following sintering temperatures were applied: WC-6Co at 1450 °C; WC-10Co at 1420 °C; WC-6Co-6Ni at 1400 °C; WC-6Co-12Ni and WC-20Co at 1360 °C.

The different steps of powder processing were monitored by scanning electron microscopy and EDS-analysis, in order to evaluate homogeneity of the mixture and to identify possible powder contamination. Voltammetric experiments were fulfilled using a potentiostat with computer based data acquisition and control and a conventional three-electrode-cell. The counter electrode was made of platinum wire. The reference electrode was AgCl/Ag and connected to the cell by a salt bridge and a Haber-Luggin capillary.

The samples were cleaned with ethylic alcohol in an ultrasonic bath and mounted in a PTFE holder, which exposed the front side of the cylindrical samples and permitted electrical contact at the back side. Tests were performed in 1N H₂SO₄ solution at room temperature. The solution was open to air. The scan rate was 10 mV/min. The start potential was -0.5 V(SHE).

Table 1. Mass of Co and Ni added to 100 g of commercial WC-6Co composite to obtain hard metals of defined compositions.

Hard metal	Addition of Ni (g)	Addition of Co (g)	Total mass of Co (g)	Total mass of Ni (g)
WC-6Co	0	0	6	0
WC-10Co	0	4.5	10.5	0
WC-6Co-6Ni	6.4	0.4	6.4	6.4
WC-6Co-12Ni	14	1	7	14
WC-20Co	0	17.5	23.5	0



(a)

3. Results and Discussion

3.1. Raw material

Figure 1 represents the commercial WC-6Co powder delivered by Alfa Aesar. It shows agglomeration of the powder particles. The particle size is clearly less than 10 μm as shown in Figure 1a. In Figure 1b the EDS analysis in the marked area of Figure 1a is shown. Only the elements Co and W are detected confirming the purity of the powder material.

The powders of the pure metals, Co and Ni, are shown in Figure 2a and b, respectively. Almost all particles seen in the micrographs have less than 10 μm.

The powders of WC-6Co, pure Co and pure Ni were mixed in the quantities indicated in Table 1 as described in the Materials and Methods section.

3.2. Characterization of powder mixtures

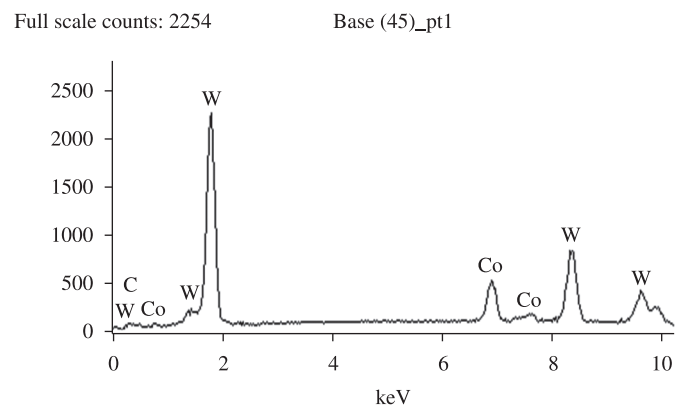
The powder mixtures were analyzed by scanning electron microscopy in order to evaluate the degree of homogeneity obtained by the mixing procedure. Figure 3a and 3b show the mixtures of the WC-10Co and WC-20Co composites, respectively. In Figure 3a agglomerated WC-6Co particles of grey color can be distinguished from agglomerated Co particles which are darker. White particles of lubricant can also be identified. The powder mixture of the WC-20Co composite in Figure 3b shows a much more homogeneous distribution of the powders and the lubricant.

The powder mixture for WC-6Co-6Ni in Figure 4a shows good homogeneity, since none of the constituents can be identified separately. In the case of the WC-6Co-6Ni mixture (Figure 4b) agglomerated Ni as well as agglomerated and isolated WC-6Co particles are visible. Pure Co cannot be identified due to its low amount in the sample.

After the described mixing procedure the apparent density of the powder mixtures were determined. Table 2 shows that the commercial WC-6Co powder has the highest apparent density and the value diminishes with the growing quantity of binder phase.

3.3. Powder compacting

The powders were pressed in a cylindrical die with a compacting pressure of 200 MPa. The highest green density is obtained with the commercial WC-6Co powder. The green density is lowered as the binder content grows (Table 3).



(b)

Figure 1. a) Micrograph of WC-6Co-powder. b) EDS of selected area in Figure 1a.

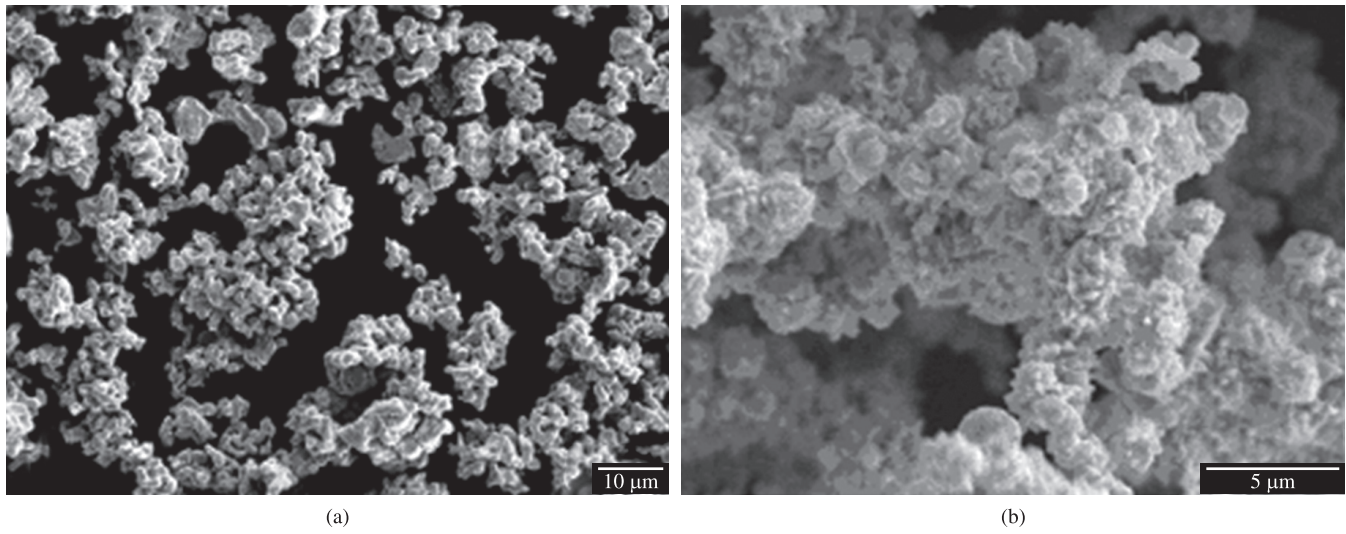


Figure 2. a) Micrograph of pure Co-powder. b) Micrograph of pure Ni-powder.

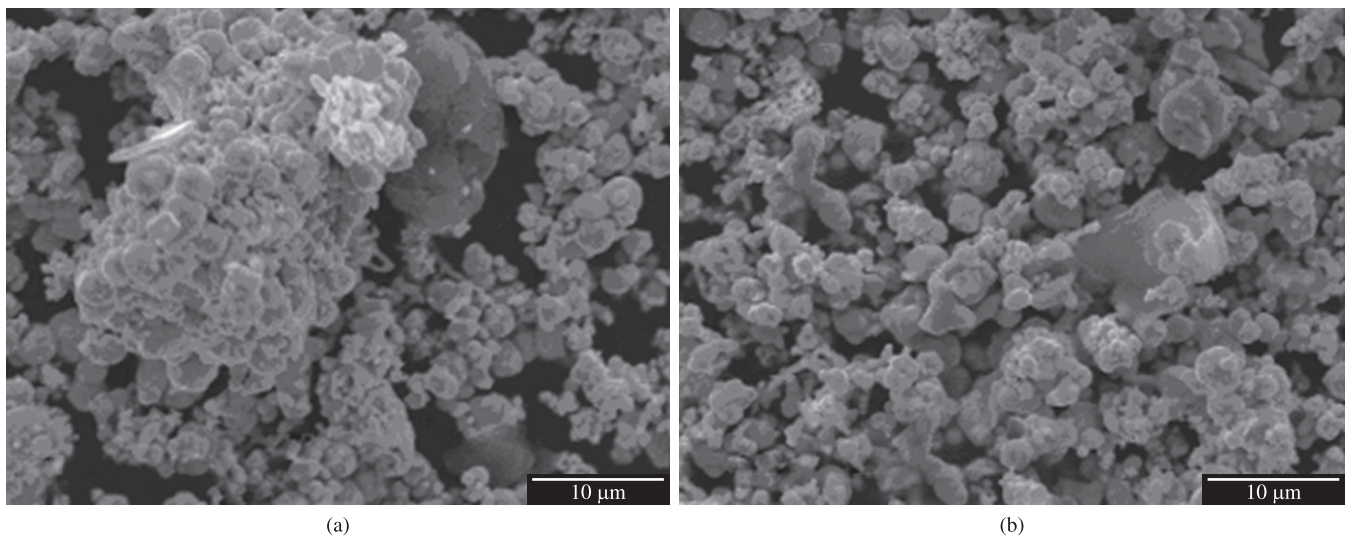


Figure 3. a) Micrograph of WC-10Co. b) Micrograph of WC-20Co.

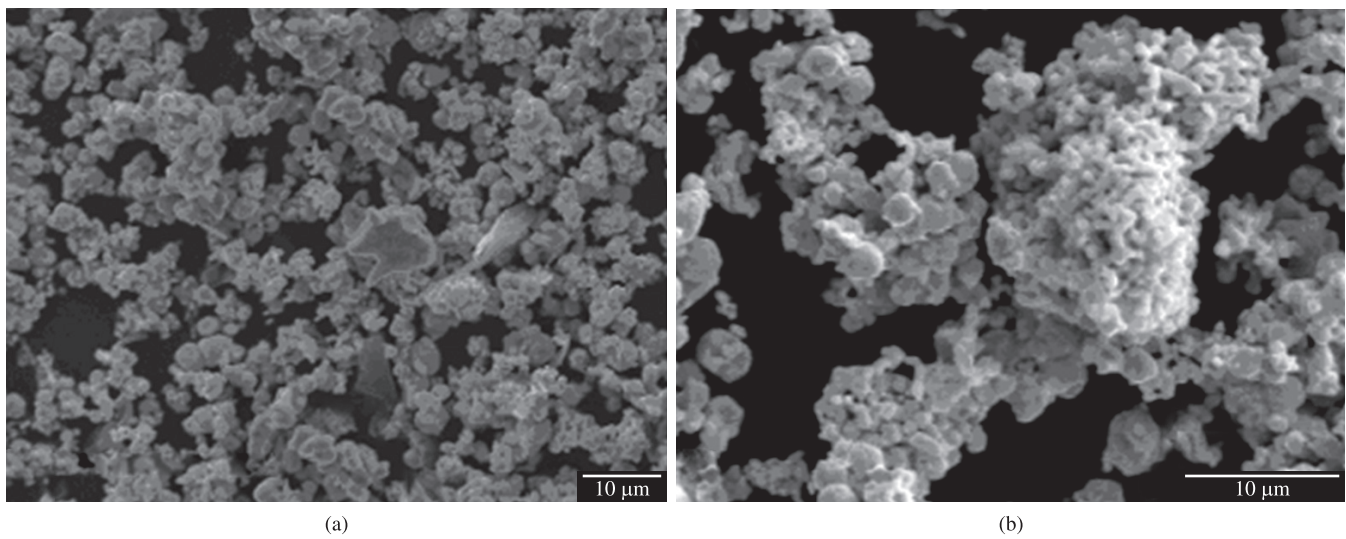


Figure 4. a) Micrograph of WC-6Co-6Ni. b) Micrograph of WC-6Co-12Ni.

3.4. Sintered hard metals

After the sintering treatment described above, the density of the sintered hard metals was determined by Arquimedes' principle, in accordance with the MPIF-95 norm (Table 4). With increasing binder phase contents lower relative densities were determined. Also, the comparison of WC-6Co-12Ni and WC-20Co indicates that Ni in the binder phase lowers the relative density.

Volumetric and linear contractions of the hard metal are compared in Table 5. Radial contraction was smaller than axial contraction, since the latter is more strongly influenced by variations of compacting pressure, temperature and duration of sintering.

Sintered alloys were studied by scanning electron microscopy, which revealed the microstructure better than light microscopy with Murakami attack. Electron microscopic studies showed that sintering of the WC-6Co and WC-10Co powders (Figure 5) led to a homogeneous distribution of the carbide particles and the Co binder

phase. Diffusion between carbides and grain growth was observed. Small islands of Co are present in the WC-10Co material. EDS analysis showed only the presence of elements from the raw materials. No sign of contamination by the production process was detected (Figure 6). This applies to all compositions studied.

The microstructure of the Ni-containing samples differs from the Ni-free ones (Figure 7). A finer and more homogeneous distribution

Table 2. Apparent density of the hard metals.

Composition of hard metal	Apparent density (g.cm ⁻³)
WC-6%Co	2.63 ± 0.02
WC-10%Co	2.57 ± 0.04
WC-6%Co6Ni	2.55 ± 0.03
WC-6%Co12Ni	2.47 ± 0.03
WC-20%Co	2.45 ± 0.02

Table 3. Green density of the compacted hard metals.

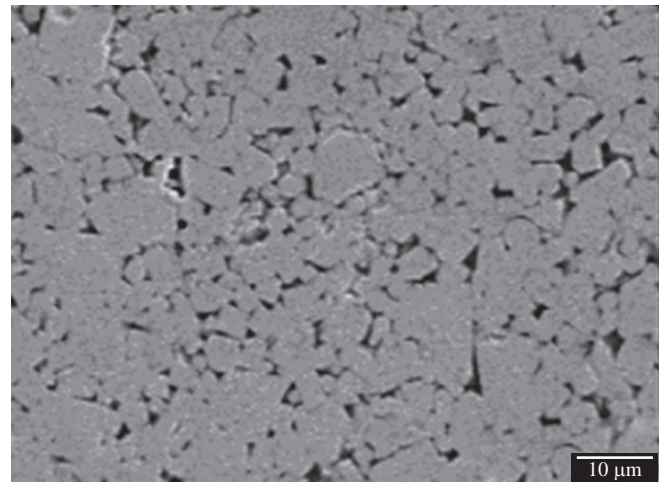
Composition	Green density (g.cm ⁻³)
WC-6Co	8.02 ± 0.13
WC-10Co	7.80 ± 0.16
WC-6Co-6Ni	7.62 ± 0.19
WC-6Co-12Ni	7.11 ± 0.18
WC-20%Co	7.03 ± 0.12

Table 4. Density of sintered hard metals.

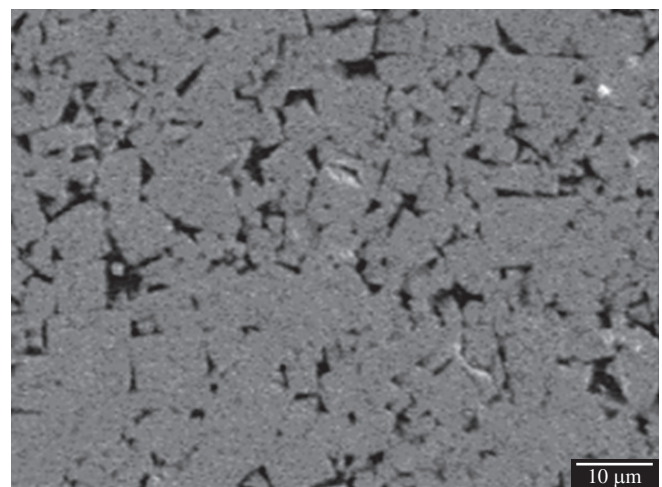
Composition of hard metals	Density of sintered materials (g.cm ⁻³)	Theoretic density (g.cm ⁻³)	Relative density (%)
WC-6Co	14.64 ± 0.06	14.90	97.8 – 98.6
WC-10Co	14.19 ± 0.16	14.60	96.1 – 98.3
WC-6Co-6Ni	13.40 ± 0.21	14.30	92.3 – 95.2
WC-6Co-12Ni	13.05 ± 0.21	13.76	93.3 – 96.4
WC-20Co	13.13 ± 0.14	13.60	95.5 – 97.6

Table 5. Volumetric and linear contraction of the hard metals.

Composition of hard metal	Volumetric contraction (%)	Linear contraction (height) (%)	Linear contraction (diameter) (%)
WC-6Co	43.6 – 48.6	17.2 – 19.3	19.0 – 19.8
WC-10Co	43.8 – 47.8	17.1 – 19.3	19.0 – 19.8
WC-6Co-6Ni	43.6 – 48.7	17.3 – 19.5	19.0 – 19.7
WC-6Co-12Ni	44.1 – 48.7	17.3 – 19.5	18.9 – 19.8
WC-20Co	43.8 – 48.5	17.3 – 19.4	19.0 – 19.8



(a)



(b)

Figure 5. a) WC-6Co, sintered at 1450 °C. b) WC-10Co sintered at 1420 °C.

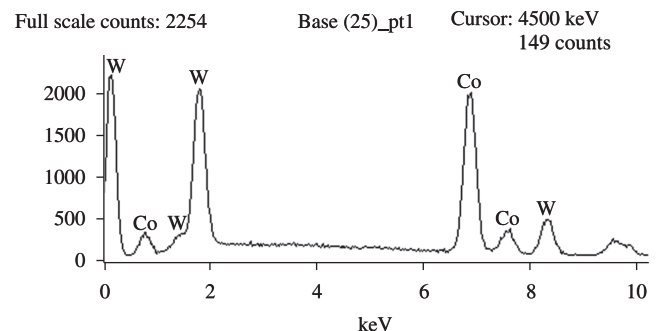


Figure 6. EDS analysis of WC-10Co sintered at 1420 °C.

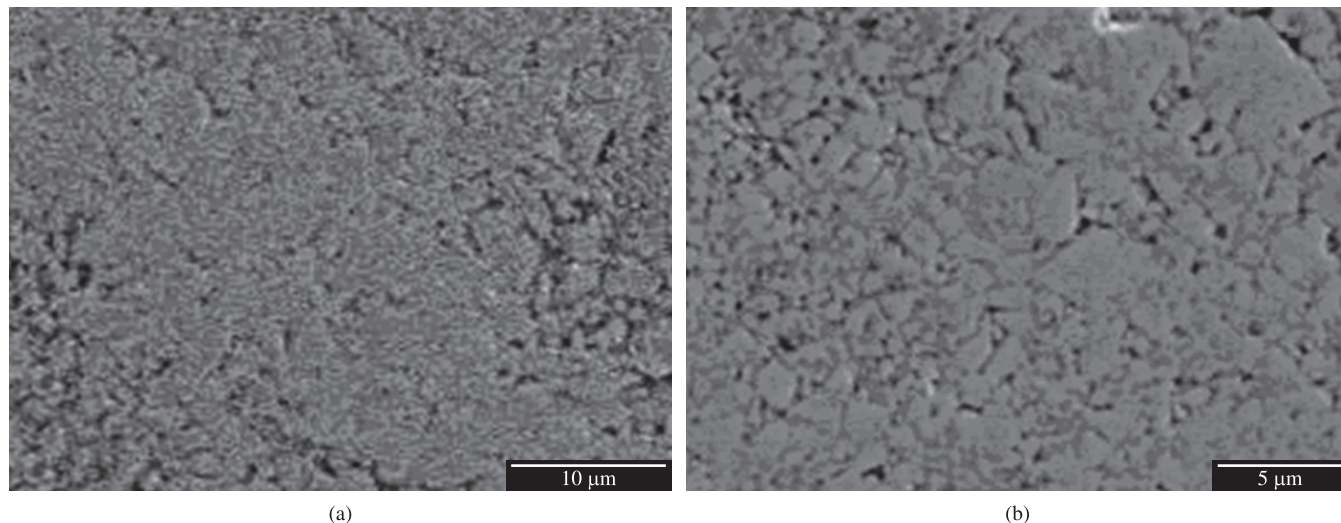


Figure 7. a) WC-6Co-6Ni sintered at 1400 °C. b) WC-6Co-12Ni sintered at 1360 °C.

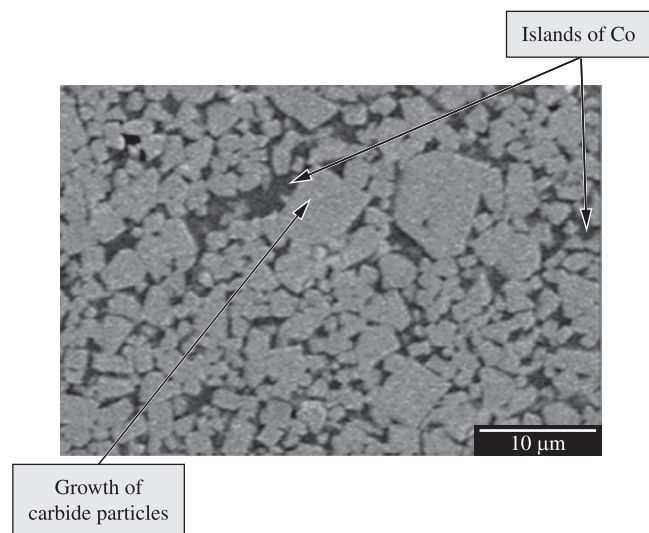


Figure 8. Sem of WC-20Co sintered at 1360 °C.

of carbides and of Ni and Co binder was found, especially in the WC-6Co-6Ni material (Figure 7a). No distinction between Co and Ni binder could be made, nor could be detected islands of Co or Ni, despite of a total binder content of 12%. Small islands of binder phase were found in WC-6Co-12Ni. Growth of carbide particle up to more than 10 μm can be observed in some parts of the specimen (Figure 7b).

The sintered WC-20Co shows islands of Co and growth of carbide particles, some of them reaching about 10 μm (Figure 8). Due to the higher binder content WC particles are completely surrounded by Co.

3.5. Electrochemical behavior

Potentiodynamic tests in H₂SO₄ were performed in order to get an overview of the electrochemical behavior of the sintered hard metals. Figure 9 compares the curves as a function of the Co-binder content. The cathodic curves are nearly identical for the three compositions studied. The same observation was made with respect to the anodic Tafel lines. Therefore the corrosion potentials of the three hard metals are similar. At higher anodic potentials WC20Co reaches a

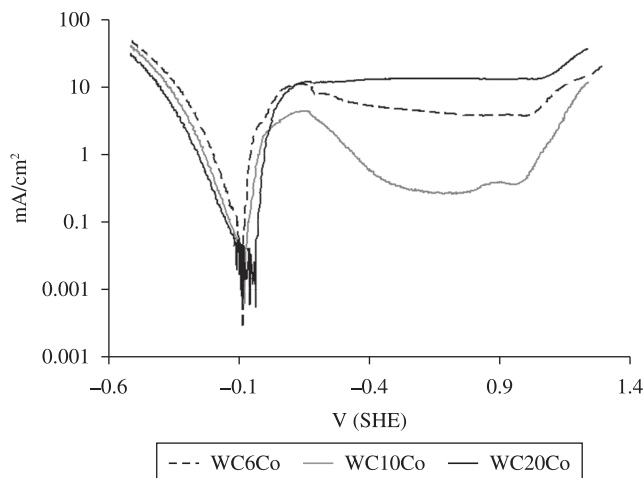


Figure 9. Potentiodynamic curves of hard metals as a function of Co-binder content.

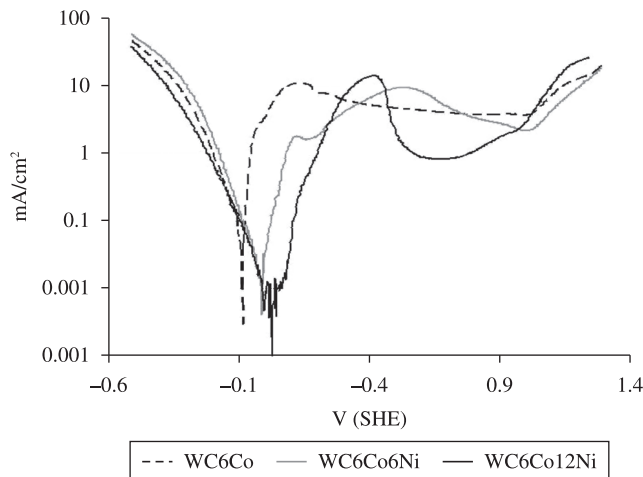


Figure 10. Potentiodynamic curves of hard metals as a function of Ni-content in the binder.

current density plateau of about $10 \text{ mA}\cdot\text{cm}^{-2}$. With lower Co content the current density in the anodic potential region becomes smaller. However, WC10Co showed a lower current density than WC6Co, which indicates that other parameter than the binder content might have an influence. This question is also controversially discussed in the literature. Some works report lower current densities with lower binder content¹³, while others found that the binder content has no influence¹⁴. Also, others report that the current density depends on the carbide grain size¹⁵.

Figure 10 compares hard metals with different Ni contents. The cathodic curves show a small influence of the Ni content. The anodic curves, however, are shifted to higher potentials with growing Ni content. Therefore, the corrosion potential is also shifted to higher potentials and the corrosion current density becomes smaller with growing Ni content. At higher anodic potentials current densities remain high in all examined materials. Transpassive behavior begins above approximately +1 V.

4. Conclusions

The powder metallurgical production route of WC-Co and WC-CoNi hard metals, starting from a commercial WC-6Co powder, gave satisfactory results for the analysed compositions: WC-10Co, WC-20Co, WC-6Co-6Ni and WC-6Co-12Ni. A homogeneous distribution of the added Co and Ni powders was found, showing that the mixing, milling, compacting and sintering procedures were performed with adequate parameters. No contamination with elements other than the constituents of the raw materials was detected by EDS analysis.

A comparison of sintered density and sintering temperature of the examined alloys shows that sintering temperature is the main factor which determines the density. The highest sintered density was obtained with the commercial WC-6Co powder which was sintered at the highest temperature. In the case of WC-6Co the different production process of the commercial material might also have an influence on the results. The comparison of WC-6Co-12Ni and WC-20Co indicates that Ni in the binder phase tends to lower the relative density.

Carbide grain growth was observed in all sintered materials, however, a finer distribution of the constituents, WC particles and Co-Ni binder phase, was found in the composition WC-6Co-6Ni.

In the potentiodynamic corrosion tests in sulfuric acid all materials showed a behavior described sometimes as “pseudo-passive”¹⁶, which means that the current density in the passive range remains high due to non-adherent, non-protecting corrosion products. The Ni-containing hard metals showed a shift of the anodic curve of metal dissolution, indicating a decrease of the corrosion current density with growing Ni content in the binder.

Acknowledgements

The authors gratefully acknowledge financial support by FINEP and by IMER Usinagem Porto Alegre - RS.

References

1. Silva AGP. The Role of Bender Phase in The WC-Co Sintering. *Materials Research*. 2001; 4(2):59-62. <http://dx.doi.org/10.1590/S1516-14392001000200003>
2. Rodrigues MF, Bobrovnichii GS, Quintanilha R, Cândido R, Silva G and Filgueira M. Sinterização da Liga WC/10Co Por Altas Pressões. *Revista Matéria*. 2006; 11(3):174-180.
3. Thümmel F and Oberacker R. *An introduction to powder metallurgy*. Cambridge, Great Britain: The Institute of Materials; 1993. p. 280-285
4. Schäfer F, Kolaska H and Grewe H. *Hartmetallwerkzeuge im Bergbau*: Pulvermetallurgie der Hartmetalle. Deutschland: FPM-Fachverband Pulvermetallurgie, 1992. Kapitel 15.
5. Gomes UU, Buriti AC and Silva AGP. Computer Modelling of WC Crystallite Cross Section Distribution in WC-Co Hardmetal Grade. In: *Powder Metallurgy World Congress*; 1998; Granada, Espanha. Granada: European Powder Metallurgy Association; 1998.
6. Phase diagram. Available from: <http://www.infomet.com.br/diagramas-fases-ver.php?e=mostrar&jd_diagrama=120&btn_filtrar=ok>. Access in: 25/12/2010.
7. Machado FAL, Filgueira M, Esquef I, Vargas H and Faria Junior RT. Caracterização térmica, estrutural e mecânica da liga de Metal duro WC-10 % Co. In: *Anais do 17º Congresso Brasileiro de Engenharia e Ciência dos Materiais – CBECIMat*; 2006, Foz do Iguaçu, Brasil. Foz do Iguaçu: IPEN; 2006.
8. Available from: <<http://www.webelements.com/cobalt/>>. Access in: 24/11/2009.
9. Crook P. Corrosion of Cobalt-Base Alloys. In: *ASM Metals Handbook: Properties and Selection Nonferrous Alloys and Special Purpose Materials*. 9th ed. Washington: ASTM; 1998. vol. 2, p. 1404-1406.
10. Cemented Carbides. Powder Metallurgy Cermets and Cemented Carbides. In: *ASM Metals Handbook: Powder Metal Technologies and Applications*. 9th ed. Washington: ASM International; 1998. vol. 7, p. 2337.
11. Chiaverini V. *Metalurgia do pó*. 4th ed. São Paulo, Brasil: Associação Brasileira de Metalurgia e Materiais-ABM; 2001. p. 184-187.
12. Paganini PP. *Síntese e caracterização de trocadores iônicos inorgânicos a base de óxidos mistos estanho-titânio para utilização na recuperação de cádmio e níquel e estudos fotoluminescentes*. [Dissertação]. São Paulo: Instituto de Pesos e Medidas; 2007.
13. Human AM and Exner HE. Electrochemical Behavior of Tungsten-Carbide Hard Metals. *Materials Science and Engineering: A*. 1996; 209:180-191. [http://dx.doi.org/10.1016/0921-5093\(95\)10137-3](http://dx.doi.org/10.1016/0921-5093(95)10137-3)
14. Human AM and Exner HE. The relationship between electrochemical behaviour and in-service corrosion of WC based cemented carbides. *International Journal of Refractory Metals and Hard Materials*. 1997; 15:65-71. [http://dx.doi.org/10.1016/S0263-4368\(96\)00014-5](http://dx.doi.org/10.1016/S0263-4368(96)00014-5)
15. Tomlinson WJ G and Ayerst J. Anodic polarization and corrosion of WC-Co hardmetals. *Journal Materials Science*. 1989; 24:2348-2354. <http://dx.doi.org/10.1007/BF01174495>
16. Sutthiruangwong S, Mori G and Kösters R. Passivity and pseudopassivity of cemented carbides. *International Journal of Refractory Metals and Hard*. 2005; 23:129-136. <http://dx.doi.org/10.1016/j.ijrmhm.2004.11.006>